Materials Advances

ROYAL SOCIETY OF CHEMISTRY

PAPER

View Article Online
View Journal | View Issue

Cite this: *Mater. Adv.*, 2023, 4, 1075

Porous recyclable sponges with controllable and durable shape memory†

Jinfeng Cao, Cong Gui and Shengyu Feng *

In recent years, porous shape memory polymers (SMPs) with morphological and functional diversity, durability, flexibility, and recyclability are substantially required because of the increasingly demanding applications. In this study, a porous silicone sponge with exquisite structures, and controllable and durable shape memory property is designed and synthesized by a one pot click reaction, which can respond to two kinds of stimuli including heat and solvent. The sponge can be degraded and the products are used as raw materials for the synthesis of a sponge again, indicating its application potential in green chemistry. The sponge also has high- and low-temperature resistance, and can remove organic solvents from water. After coordination with Eu^{3+}, the elasticity of the sponge is significantly improved and the shape memory ability disappears, and fluorescence of the sponge under 365 nm UV light changes from blue to red meanwhile. Due to the good biocompatibility of silicone-based materials, they are expected to be used in the medical and health care fields.

Received 5th October 2022,
Accepted 4th January 2023

DOI: 10.1039/d2ma00953f

rsc.li/materials-advances

Introduction

Smart materials, as a kind of novel materials in the modern scientific research field, have attracted extensive attention and developed into an interdisciplinary subject due to their unique functions such as integrated sensors, actuators and control systems.[1–3] They play an important role in the development and progress of human science.[4,5] Shape memory polymers (SMPs) are an important subclass of smart materials, and they can recover from a deformed shape back to the original shape due to external stimuli such as heat, light, electricity, magnetic field, water and solvents.[6–8] SMPs possess many advantages over the traditionally existing shape memory alloys, such as high shape recovery, lightness, easy manufacturing, low cost, adjustable physical properties by small changes in chemical composition and structure and so on, resulting in potential substitutes for alloys, leading to potential applications in diverse ranges of areas including robotics, biomedical engineering, aerospace and automotive industries, and tactile devices.[9–13]

Compared with the traditional nonporous SMPs, porous SMPs including sponges possess lower density, higher specific strength, specific modulus and compressibility, providing additional capabilities such as the highlight deformation ability up to 1000% and energy dissipation.[14,15] In addition, the characteristics of large compression and recovery can endow the materials with the self-healing function. When the material is impacted by external compression rather than fracture type damage, it can repair itself and return to its original shape after the corresponding stimulus. Furthermore, the shape memory sponge can also be compressed to a small volume to greatly save space and transportation cost. After arriving at the destination, the shape memory sponge will be restored from the deformation without affecting the use.[16–19] Last but not least, the porous SMP sponges are flexible and have been widely used in the fields of packaging, sensors, and intelligent medical devices.[20–22] For example, Kaplan *et al.* designed porous silk protein sponges with wonderful shape memory characteristics and volumetric recovery following compression, which were useful for minimally invasive deployment in soft tissue augmentation.[23] Jiang *et al.* reported a superlyophilic porous shape memory sponge with tunable pore size, and precisely tunable permeation flux was obtained while the rhodamine B was accurately released.[24] Ye *et al.* fabricated ultra-lightweight polyurethane foams with adjustable EMI shielding and shape memory functions by using a conductive carbon nanotube polymer composite layer and a crystallized paraffin layer, and the shape changed *via* an external stimulus to adjust the EMI shielding efficiency autonomously.[25]

Recently, porous SMPs with more morphological diversity, functionality and better durability are substantially required in our daily lives, and the increasingly demanding applications call for continuous innovation.[26–28] Degradable green materials

Key Laboratory of Special Functional Aggregated Materials & Key Laboratory of Colloid and Interface Chemistry (Shandong University), Ministry of Education, Shandong Key Laboratory of Advanced Organosilicon Materials and Technologies, School of Chemistry and Chemical Engineering, Shandong University, Jinan 250100, P. R. China. E-mail: fsy@sdu.edu.cn

† Electronic supplementary information (ESI) available. See DOI: https://doi.org/10.1039/d2ma00953f

are more needed for the environmental considerations that could minimize pollution.[29] The ultimate goal is the SMPs that are flexible and soft, which can be used for soft robotics and smart wearable devices.[30–32] Silicone sponges are silicone-based polymers with 3D network structures, possessing high flexibility, porosity, adiabaticity, high and low temperature resistance, weather resistance, radiation resistance, electrical insulation, physiological inertia, and biocompatibility, which can be used in extreme or special fields.[33–35] They can be degraded under mild conditions, and the degraded products can be used in the next polymerization.[36–38] However, there are currently no shape memory silicone sponges yet.[39] In this paper, a novel porous shape memory silicone sponge was fabricated by a one pot thiol-ene click reaction with the shape memory property in the ambient environment, and response to two kinds of stimuli. It can be made into complicated shapes by adjusting the mold shape, and can be repeatedly pressed/recovered based on the good shape memory property. Its shape memory property is also adjustable by changing the reaction condition.

Results and discussion

2.1 Characteristics of the SS-COOH

The silicone sponge SS-COOH was prepared by a one pot thiol-ene click reaction in a frozen emulsion within 30 min, which was much more efficient than the traditional methods to prepare the silicone sponges by vulcanization foaming of silicon rubber.[40,41] Generally, freezing polymerization involves the formation of solvent crystals (as a temporary template and porogen) within a reactant mixture, followed by polymerization or crosslinking between these preformed polymers.[21,42] The freezing polymerization of the $PD^{Vi}MS$ in the emulsion resulted in unique pore structures with dense pore walls as shown in the SEM image (Fig. 1a). Determined by mercury porosimetry, the SS-COOH exhibited a wide pore diameter distribution from about 1 to 40 μm with an average pore diameter of 1.32 μm (Fig. 1b). The SS-COOH possessed a high porosity of 74.88%, and a low density of 0.2648 g mL^{-1}. The SS-COOHs with different exquisite constructions (whale and bear) were obtained by mold forming and demoulding directly, indicating the easy morphological diversity by a simple method (Fig. 1c).

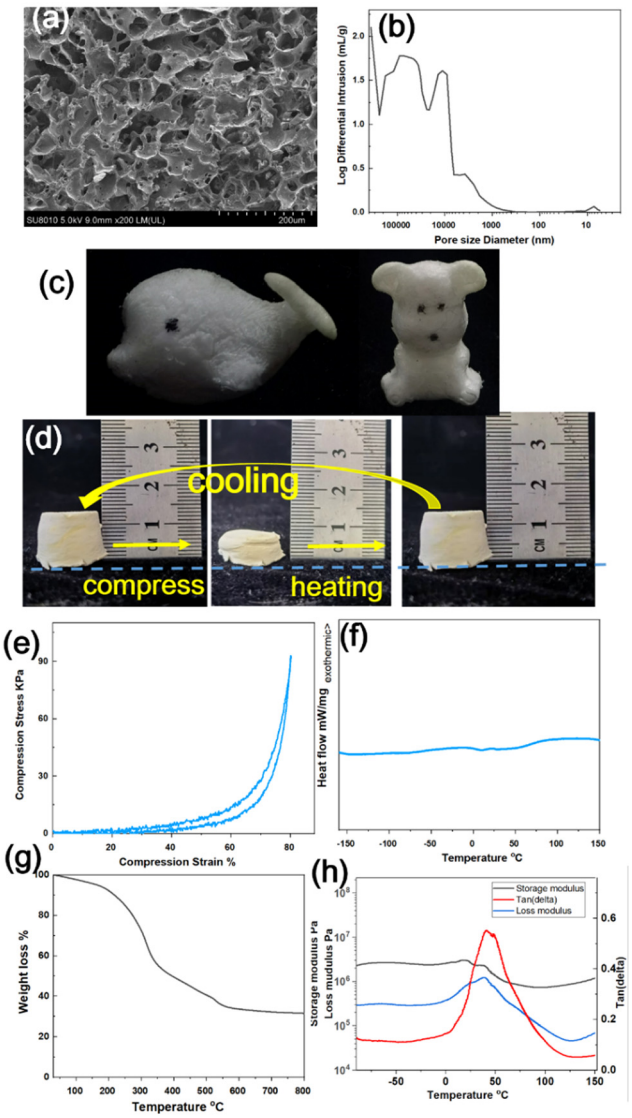

Fig. 1 (a) SEM image, and (b) pore size distribution obtained by mercury porosimetry of the SS-COOH. (c) The sponge whale and bear; (d) the shape memory property photograph of the SS-COOH before and after compression at room temperature and heating at 90 °C after about 1 min. (e) Compressive stress–strain curve under 80% strain of the SS-COOH at 90 °C. (f) DSC curve from −150 to 150 °C under N_2 at 10 °C min^{-1} of the SS-COOH and (g) TGA curves of SS-COOH under air at 10 °C min^{-1}. (h) DMA curve of the SS-COOH.

2.2 The shape memory properties of the SS-COOH

Furthermore, the SS-COOH could be compressed easily at room temperature (25 °C), and fix the compressive deformation of ~20% quickly (Fig. 1d). The as-formed deformation could be well kept at room temperature without an external force. The deformed SS-COOH could recover to the original thickness after being placed in a drying oven at 90 °C for ~1 min (Fig. 1d). It possesses the quick rebound property at >90 °C, and the compressive stress–strain curve is shown in Fig. 1e. The compressive stress is 91 kPa at 80% strain, and it is not collapsed during the substantial compression. The compression process almost did not affect the porosity and pore size distribution (Fig. S1a, b, ESI†), indicating good compression properties and soft tactile characteristics. The SS-COOH could restore the shape memory property again after cooling to the room temperature. This shape memory process based on temperature was repeated 20 times, while the shape memory property was perfectly maintained, indicating the good durability of the shape memory property of the sponge.

The glass-transition temperature (T_g) of the SS-COOH was 60 °C, obtained by DSC curve shown in Fig. 1f, and the broad temperature range of glass-transition was assumed to be the main cause of the shape memory property resulting from the interplay between carboxylic acid groups. The glass transition

was the only thermal event observed from −160 to 150 °C, suggesting that the SS-COOH was a single-phase amorphous material, which also proved the high and low temperature resistance property. The heat resistance property was also confirmed by the TGA curve recorded in air shown in Fig. 1g, and it displayed a 5% weight loss at 165.8 °C, and the residual weight was 31.5% after heating to 800 °C. When the silicone-based sponge material burns, a layer of silica forms on the outer layer, preventing further burning and thus preventing the fire from spreading.[43,44] Fig. 1h shows a representative DMA curve of the SS-COOH. The tan δ peak was very broad, showing a 10 °C to 80 °C range over 0.2, indicating that the sponge provided a good damping effect over a broad temperature range. The combination of crosslinking and a glass-transition endowed the sponge with shape memory characteristics.

Besides the thermally induced shape memory function, solvent-induced shape recovery could also be achieved. As shown in Fig. 2a, the SS-COOH in a compressed shape recovered to its largely expanded volume *via* exposure to dichloromethane dyed with oil red O. With the solvent-induced shape recovery process, dichloromethane was absorbed into the sponge. The entire shape memory and recovery process was fast and repeatable, taking less than half a minute. However, it remained the compressed shape when immersed in water (Fig. 2b), showing the selective solvent response properties. The selective organic solvent-induced shape memory principle was that the sponge had different affinity for different liquids. It was hydrophobic, and the contact angle was 125.3° (Fig. S1c, ESI†). The contact angle of the sponge for dichloromethane, kerosene, toluene, ethanol, acetone, and cyclohexane was all 0° (Fig. S1d, ESI†). Furthermore, the SS-COOH can also adsorb many other organic solvents from water, such as kerosene, toluene, ethanol, acetone, cyclohexane and so on, with adsorption ability from 300–800% (Fig. 2c), and it also has good reusability using dichloromethane as the example (Fig. 2d).

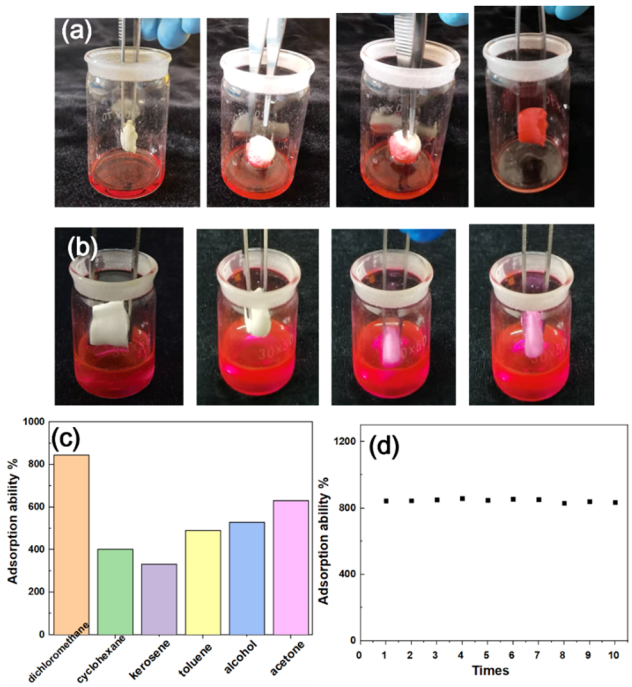

Fig. 2 The photographs of (a) dichloromethane-induced shape recovery, and (b) no shape recovery effect when immersed in water for the SS-COOH. (c) The adsorption ability of the SS-COOH for different kinds of solvents. (d) The adsorption reusability of the SS-COOH for solvents using dichloromethane as the example.

2.3 The recyclability of the SS-COOH

The recyclability of the SS-COOH was implemented in two main steps. First, the SS-COOH was degraded in an alkaline environment, and then the product was used to synthesize the raw material ($PD^{Vi}MS$) for the reproduction of SS-COOH (Fig. 3a). The degradation product mainly contains Si–CH_3 and Si–CH═CH_2 as shown in the ^{1}H NMR spectra (Fig. 3b). It was used for the synthesis of the polymer $PD^{Vi}MS$-1 (the main chain contains Si–CH_3 and Si–CH═CH_2) by anionic polymerization,

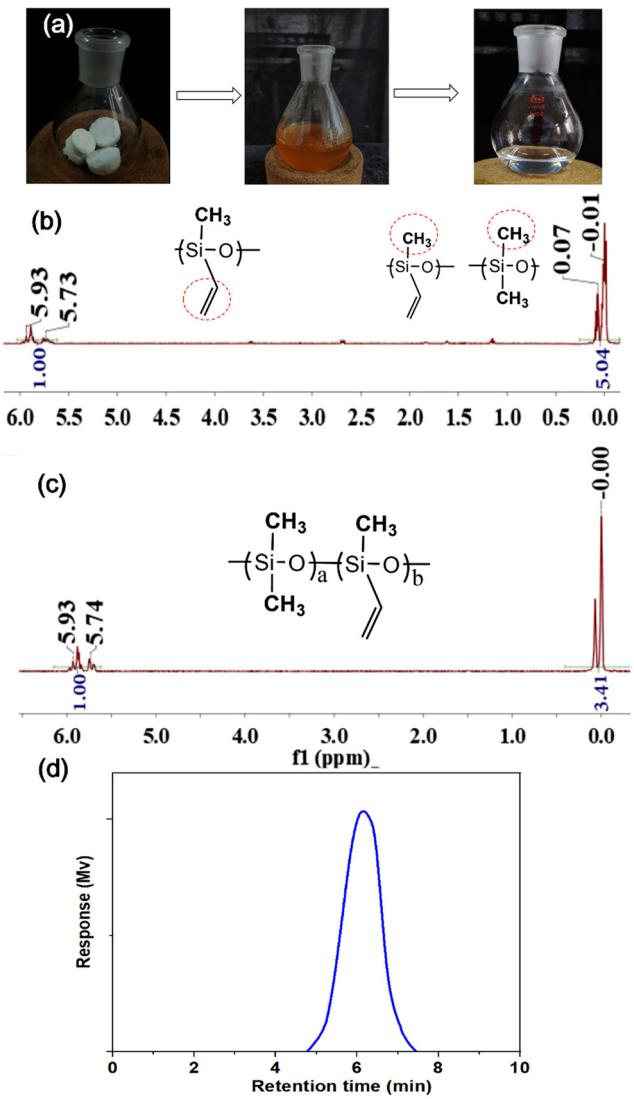

Fig. 3 (a) The photographs of the degradation process for the SS-COOH. The ^{1}H NMR spectra of (b) the degradation product and (c) the polymer $PD^{Vi}MS$-1. (d) The GPC spectra of the $PD^{Vi}MS$-1.

which is characterized in Fig. 3c. The GPC data show the M_n of 108 010 g mol^{-1}, M_w of 280 516 g mol^{-1}, M_z of 685 075 g mol^{-1}, and PDI of 2.59713 (Fig. 3d), proving the successful recyclability of the sponge.

2.4 Properties of the SS-Eu

In order to prove the T_g cause of the shape memory property, the europium ion Eu^{3+} was added into the SS-COOH, and the SS-Eu was obtained after coordination between Eu^{3+} and the –COOH group in SS-COOH. XPS shows that there are only four kinds of elements in SS-COOH, including Si, O, C, and S (Fig. 4a), while there are six elements in SS-Eu, including Si, O, C, S, Eu, and N (Fig. 4b). The binding energy of the C 1s and O 1s both decreased after the Eu^{3+} was added, because getting the electron could reduce the binding energy, which proved the coordination between Eu^{3+} and –COOH (Fig. S2a, b, ESI†). The elemental analysis also indicated the successful synthesis of the material (Table S1, ESI†). In addition, the FTIR analysis showed that after the coordination between –COOH groups and Eu^{3+}, the integral area of the peak at 1716 cm^{-1} (which was assigned to –C═O in COOH) became smaller, indicating that coordination occurred between –COOH groups and Eu^{3+} (Fig. 4c).[45,46] Absorption peaks at 1575 and 1381 cm^{-1} confirmed the presence of $-NO_3$ in the SS-Eu.[47,48] The Si–O–Si peak did not change in the sponge, indicating that the introduction of Eu^{3+} had no effect on the main chain. The SEM (Fig. 4d) and mercury porosimetry data (Fig. S2c, ESI†) showed that the morphology and pore structure of the sponge almost did not change, but it was found that the elasticity of SS-Eu was improved and the shape memory property disappeared. As shown in Fig. 4e, the compressive stress (0.33 MPa) of the SS-Eu under 80% compression strain was significantly stronger than that of the SS-COOH, and the maximum stress was almost unchanged after repeated 5 times compression. The sponge changed from shape-memory at room temperature to high rebound. Furthermore, after coordination, the fluorescence of the sponge under 365 nm UV light changed from blue to red (Fig. 4f). Since the pore structure did not change, it was assumed that the change was caused by the increase of crosslinking density and the decrease of glass transition temperature caused by supramolecular coordination. DSC also confirmed this assumption, and the glass transition temperature was 60 °C for the SS-COOH, while there was no thermal event from −150 to 200 °C for the SS-Eu (Fig. 4g). The heat stability was also improved after the coordination, which was confirmed by the TGA curve recorded in air shown in Fig. 4h, and it displayed a 5% weight loss at 167.2 °C, and the residual weight was 54.0% after heating to 800 °C.

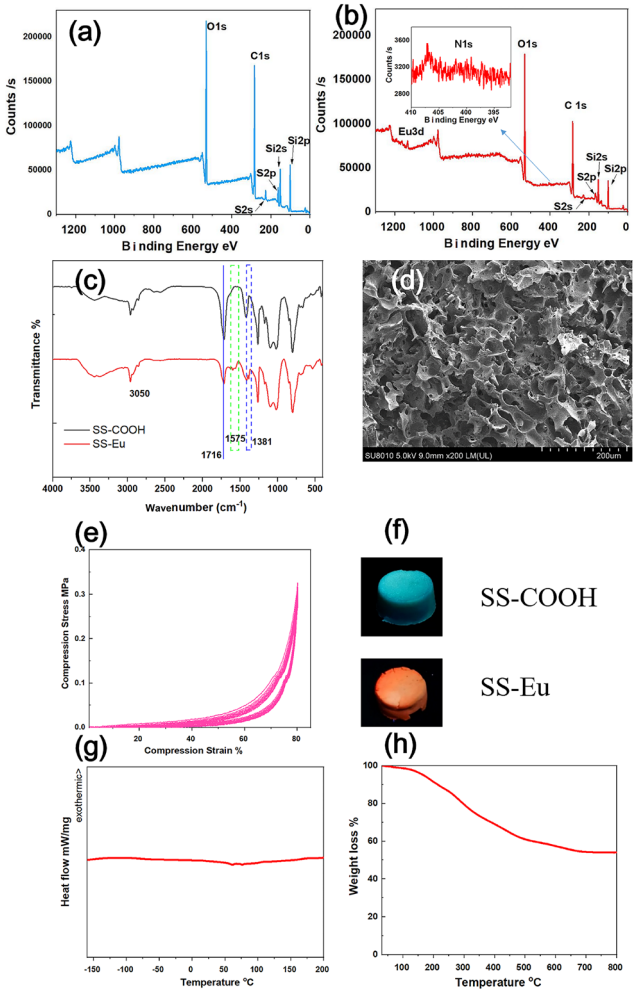

Fig. 4 XPS spectra of the (a) SS-COOH, and (b) SS-Eu. (c) Infrared spectra of SS-COOH and SS-Eu. (d) SEM image, and (e) compressive stress–strain curves under 80% strain for 5 cycles of the SS-Eu. (f) Fluorescent images of SS-COOH and SS-Eu under UV light at 365 nm. (g) DSC under N_2 and (h) TGA curves under air of the SS-Eu at 10 °C min^{-1}.

Experimental

3.1 Material and methods

Mercaptosuccinic acid (MSA), 2,2-dimethoxy-2-phenylacetophenone (DMPA), Span80, and 1,6-hexanedithiol were purchased from Sigma-Aldrich and used as received. Octamethylcyclotetrasiloxane (D_4), tetramethyl tetravinyl cyclotetrasiloxane (D_4^{Vi}), hexamethyldisiloxane (MM) and tetramethylammonium hydroxide were purchased from Shanghai Macklin Biochemical Co., Ltd as commercial products and used as received. Dichloromethane, cyclohexane, toluene, kerosene, ethanol, acetic acid, DMF, acetone, and tetrahydrofuran (THF) were purchased from Fuyu Co., Ltd.

^{1}H NMR and ^{13}C NMR spectra were obtained on a Bruker AVANCE 300 spectrometer at 298 K in $CDCl_3$. FTIR spectra were recorded on a Bruker TENSOR27 infrared spectrophotometer in the range 4000–400 cm^{-1} using KBr pellets. Gel permeation chromatography (GPC) measurements were performed in THF (1 mL min^{-1}) at 313 K with a Waters 515 HPLC (Milford, MA), equipped with a refractive index detector 2414. Scanning electron microscopy (SEM) images were obtained using a Hitachi S-4800 (7 kV). The samples were cut into small pieces and coated with a thin layer of platinum before scanning. The porous properties were characterized by Hg porosimetry using a Micromeritics Tristar 3020 instrument and a Micromeritics AutoPore IV 9500. Differential scanning calorimetry (DSC)

curves were obtained on a Netzsch DSC 204 Phoenix under an inert (N_2) atmosphere at a heating rate of 10 K min^{-1}. Elemental analyses were carried out using an Elementar Vario EL III elemental analyzer. Thermogravimetric analyses (TGA) were performed using a Mettler Toledo SDTA-854 TGA system heated to 800 °C at a heating rate of 10 °C min^{-1} under an air atmosphere. Compression tests of the sponges were performed at a loading speed of 15 mm min^{-1}, and the results were analyzed using a WDW-5 universal testing machine (China) based on ASTM D412 and ISO 527 at room temperature. The thiol-ene reaction was carried out *via* irradiation using UV light from a Spectroline Model SB-100P/FA lamp (365 nm, 100 W). The UV intensity was 4500 μW cm^{-2} at a distance of 38 cm.

3.2.1 Synthesis of $PD^{Vi}MS$. $PD^{Vi}MS$, a colorless liquid, was prepared with a yield of 86% in our own lab by a classical method.[40,41] D_4 (25.82 g), D_4^{Vi} (20.1 g), MM (0.2 g) and tetramethylammonium hydroxide (0.01 g) were added into a 100 mL three neck flask with a stir bar and condenser under an argon atmosphere. The mixture was heated to 95 °C for 3 h after stirring at 70 °C for 30 min, and heated to 150 °C for 30 min. $PD^{Vi}MS$ was then obtained after removing volatile fractions in a vacuum at 180 °C. ^1H NMR (400 MHz, $CDCl_3$, ppm): δ = 0.07–0.14 (m, $-CH_3$), 5.83–5.95 (m, $-Ch{=}CH_2$). ^{13}C NMR (75 MHz, $CDCl_3$, ppm): 0.63–1.06 ($-SiCH_3$), 132.75–137.06 (m, $-CH = CH_2$). GPC: M_n [g mol^{-1}] = 192 131, M_w [g mol^{-1}] = 863 009, M_z [g mol^{-1}] = 2 048 260, PDI = 4.49.

3.2.2 Synthesis of the silicone sponge (SS-COOH). $PD^{Vi}MS$ (0.3 g), 1,6-hexanedithiol (0.038 g), mercaptosuccinic acid (0.38 g), cyclohexane (7.2 mL), deionized water (0.4 g), Span 80 (0.02 g) and DMPA (0.15 g, 2 wt%) were added into a dry 15 mL weighing bottle and mixed *via* magnetic stirring. The mixture was then irradiated with 100 W of UV light (λ_{max} = 365 nm) at −10 °C for 30 min. The resulting crude product was washed with tetrahydrofuran and ethanol to remove unreacted reactants, and dried by evaporation under ambient conditions. The white silicone sponge SS-COOH (0.43 g) was obtained.

3.2.3 The recyclability of the silicone sponge (SS-COOH). The recyclability of the SS-COOH included the degradation and the re-synthesis of the $PD^{Vi}MS$. The SS-COOH (10.0 g) was cut into small pieces and put into a 100 mL pear-shaped bottle with toluene (20 mL). 0.3 g of KOH was dissolved in methanol and added into the above bottle. After refluxing at 110 °C for 2 hours, acetic acid was added to quench the KOH. The product (0.96 g) was obtained by vacuum distillation at 160 °C.

The above product (0.96 g), MM (0.02 g), D_4^{Vi} (0.12 g) and tetramethylammonium hydroxide (0.01 g) were added into a 25 mL three neck flask, and the $PD^{Vi}MS$-1 was synthesized in a similar way to $PD^{Vi}MS$.

3.2.4 Synthesis of the silicone sponge (SS-Eu). The SS-COOH (0.43 g) was immersed in a tetrahydrofuran (6 mL) solution containing $Eu(NO_3)_3{\cdot}6H_2O$ (0.108 g), and then heated at 60 °C for 4 h. The product was placed in a vacuum oven for 4 h, and then washed with ethanol to obtain 0.47 g of the SS-Eu, yield 49%.

Conclusions

The porous shape memory silicone sponge was designed and synthesized for the first time by a one pot reaction within 30 min, and its T_g was 60 °C. It can respond to both heat and certain kinds of liquids. The deformation and recovery of shape can be repeated many times, indicating the good durability. The sponge also had good recyclability. Both the elasticity and fluorescence of the sponge were controllable. Due to the potential biocompatibility of silicone-based materials, the application in the medical field will be studied in the future.

Author contributions

Jinfeng Cao conceived the idea, designed the experiments and performed the analysis. Cong Gui performed the synthesis and characterization. All authors have contributed to writing the manuscript. Shengyu Feng revised the manuscript.

Conflicts of interest

There are no conflicts to declare.

Acknowledgements

This work was financially supported by the National Natural Science Foundation of China (52173102, 52103007), Shandong Provincial Natural Science Foundation (ZR2019MB028), and Fluorine Silicone Materials Collaborative Fund of Shandong Provincial Natural Science Foundation (ZR2021LFG001).

Notes and references

1 M. Su and Y. Song, *Chem. Rev.*, 2022, **122**, 5144–5164.
2 M. A. English, L. R. Soenksen, R. V. Gayet, H. de Puig, N. M. Angenent-Mari, A. S. Mao, P. Q. Nguyen and J. J. Collins, *Science*, 2019, **365**, 780–785.
3 P. Yang, F. Zhu, Z. Zhang, Y. Cheng, Z. Wang and Y. Li, *Chem. Soc. Rev.*, 2021, **50**, 8319–8343.
4 Y. Shi and Z. Chen, *J. Mater. Chem. C*, 2018, **6**, 11817–11834.
5 F. Soto, E. Karshalev, F. Zhang, B. Esteban Fernandez De Avila, A. Nourhani and J. Wang, *Chem. Rev.*, 2022, **122**, 5365–5403.
6 Y. Chen, X. Zhao, Y. Li, Z. Jin, Y. Yang, M. Yang and B. Yin, *J. Mater. Chem. C*, 2021, **9**, 5515–5527.
7 Z. Cheng, D. Zhang, X. Luo, H. Lai, Y. Liu and L. Jiang, *Adv. Mater.*, 2021, **33**, 2001718.
8 L. Cera, G. M. Gonzalez, Q. Liu, S. Choi, C. O. Chantre, J. Lee, R. Gabardi, M. C. Choi, K. Shin and K. K. Parker, *Nat. Mater.*, 2021, **20**, 242–249.
9 L. Santo, *Prog. Aerosp. Sci.*, 2016, **81**, 60–65.
10 X. Qi, H. Xiu, Y. Wei, Y. Zhou, Y. Guo, R. Huang, H. Bai and Q. Fu, *Compos. Sci. Technol.*, 2017, **139**, 8–16.
11 H. Gao, J. Li, F. Zhang, Y. Liu and J. Leng, *Mater. Horiz.*, 2019, **6**, 931–944.
12 A. Lendlein and O. E. C. Gould, *Nat. Rev. Mater.*, 2019, **4**, 116–133.
13 Y. Xia, Y. He, F. Zhang, Y. Liu and J. Leng, *Adv. Mater.*, 2021, **33**, 2000713.

14 Y. Shao, W. Hu, M. Gao, Y. Xiao, T. Huang, N. Zhang, J. Yang, X. Qi and Y. Wang, *Composites, Part A*, 2021, **143**, 106291.
15 X. Jia, B. Shen, L. Zhang and W. Zheng, *Chem. Eng. J.*, 2021, **405**, 126927.
16 H. Wu, S. Li, Y. Shao, X. Jin, X. Qi, J. Yang, Z. Zhou and Y. Wang, *Chem. Eng. J.*, 2020, **379**, 122373.
17 S. Shi, Y. Zhang, Y. Luo, X. Liao, C. Tian, W. Tang, J. Yang, J. Chen and G. Li, *Ind. Eng. Chem. Res.*, 2020, **59**, 22132–22143.
18 W. Wang, X. Liao, F. Guo, G. Wang, Z. Yan, F. Liu and G. Li, *Ind. Eng. Chem. Res.*, 2020, **59**, 7611–7623.
19 T. Wang, J. Zhao, C. Weng, T. Wang, Y. Liu, Z. Han and Z. Zhang, *J. Mater. Chem. C*, 2021, **9**, 7444–7451.
20 K. Hearon, P. Singhal, J. Horn, W. T. Small, C. Olsovsky, K. C. Maitland, T. S. Wilson and D. J. Maitland, *Polym. Rev.*, 2013, **53**, 41–75.
21 T. Wong, J. Wu, M. Yang, M. R. Abdul Kadir, M. U. Wahit and Q. Zhao, *J. Mater. Chem. A*, 2017, **5**, 9793–9798.
22 O. King, E. Constant and A. C. Weems, *ACS Appl. Mater. Interface*, 2021, **13**, 20641–20652.
23 J. E. Brown, J. E. Moreau, A. M. Berman, H. J. McSherry, J. M. Coburn, D. F. Schmidt and D. L. Kaplan, *Adv. Healthcare Mater.*, 2017, **6**, 1600762.
24 P. Liu, H. Lai, X. Luo, Q. Xia, D. Zhang, Z. Cheng, Y. Liu and L. Jiang, *ACS Nano*, 2020, **14**, 14047–14056.
25 S. Zhu, Q. Zhou, M. Wang, J. Dale, Z. Qiang, Y. Fan, M. Zhu and C. Ye, *Composites, Part B*, 2021, **204**, 108497.
26 F. Zhang, Y. Xia, Y. Liu and J. Leng, *Nanoscale Horiz.*, 2020, **5**, 1155–1173.
27 H. M. Kim, J. Park, Z. M. Huang, J. R. Youn and Y. S. Song, *Macromol. Res.*, 2019, **27**, 919–925.
28 Y. Hou, G. Fang, Y. Jiang, H. Song, Y. Zhang and Q. Zhao, *ACS Appl. Mater. Interface*, 2019, **11**, 32423–32430.
29 A. Lendlein and O. E. C. Gould, *Nat. Rev. Mater.*, 2019, **4**, 116–133.
30 S. M. Hasan, L. D. Nash and D. J. Maitland, *J. Polym. Sci., Part B: Polym. Phys.*, 2016, **54**, 1300–1318.
31 Y. Zhao, Y. Li, Q. Du, Q. Zhang, X. Lv, Q. Yang, P. R. Chang, D. P. Anderson, M. He and Y. Chen, *J. Mater. Chem. B*, 2019, **7**, 5848–5860.
32 M. F. Ahmed, Y. Li, Z. Yao, K. Cao and C. Zeng, *J. Appl. Polym. Sci.*, 2019, **136**, 47416.
33 L. Li and J. Zhang, *Nano Energy*, 2021, **81**, 105682.
34 G. Zu, K. Kanamori, A. Maeno, H. Kaji and K. Nakanishi, *Angew. Chem., Int. Ed.*, 2018, **57**, 9722–9727.
35 R. G. Jones, W. Ando and J. Chojnowski, *Silicon-containing polymers: the science and technology of their synthesis and applications*, Springer Science & Business Media, 2013.
36 A. Oku, W. Huang and Y. Ikeda, *Polymer*, 2002, **43**, 7289–7293.
37 S. Enthaler, *Angew. Chem., Int. Ed.*, 2014, **53**, 2716–2721.
38 M. Okamoto, S. Suzuki and E. Suzuki, *Appl. Catal., A*, 2004, **261**, 239–245.
39 D. Zhu, S. Handschuh-Wang and X. Zhou, *J. Mater. Chem. A*, 2017, **5**, 16467–16497.
40 J. Liu, Y. Yao, X. Li and Z. Zhang, *Chem. Eng. J.*, 2021, **408**, 127262.
41 Z. Gou, X. Zhang, Y. Zuo, M. Tian, B. Dong and W. Lin, *ACS Appl. Mater. Interface*, 2019, **11**, 30218–30227.
42 L. Li, Y. Zhang, H. Lu, Y. Wang, J. Xu, J. Zhu, C. Zhang and T. Liu, *Nat. Commun.*, 2020, **11**, 62.
43 Y. Liu, X. Wang and S. Feng, *Adv. Funct. Mater.*, 2019, **29**, 1902488.
44 C. B. Gale, B. Chin, C. Tambe, D. Graiver and M. A. Brook, *ACS Sustainable Chem. Eng.*, 2019, **7**, 1347–1352.
45 B. Li, Z. Ding, Z. Li and H. Li, *J. Mater. Chem. C*, 2018, **6**, 6869–6874.
46 X. Jia, B. Shen, L. Zhang and W. Zheng, *Chem. Eng. J.*, 2021, **405**, 126927.
47 I. K. Ortega, R. Escribano, D. Fernández, V. J. Herrero, B. Maté, A. Medialdea and M. A. Moreno, *Chem. Phys. Lett.*, 2003, **378**, 218–223.
48 A. K. Tucker-Schwartz, R. A. Farrell and R. L. Garrell, *J. Am. Chem. Soc.*, 2011, **133**, 11026–11029.